Charge transport of lithium-salt-doped polyaniline

J. H. Jung, B. H. Kim, B. W. Moon, and J. Joo*
Department of Physics and Center for Electro and Photo Responsive Molecules, Korea University, Seoul 136-701, Korea

S. H. Chang and K. S. Ryu
Electronics and Telecommunications Research Institute, Taejeon, 305-350, Korea

(Received 15 September 2000; revised manuscript received 09 March 2001; published 25 June 2001)

Charge transport properties, including temperature-dependent dc conductivity and thermoelectric power are reported for Li-salt ($LiPF_6$, $LiBF_4$, $LiAsF_6$, $LiCF_3SO_3$, or $LiClO_4$) -doped polyaniline (PAN) samples. The experiments of electron paramagnetic resonance (EPR) and X-ray photoelectron spectroscopy (XPS) are performed for the systems. The electrical and magnetic properties and the doping mechanism of various Li-salt-doped PAN samples are compared with those of hydrochloric-acid (HCl) -doped PAN samples. The PAN materials doped with $LiPF_6$ have the highest dc conductivity ($\sigma_{dc} \sim 1$ S/cm, at room temperature) in the Li-salt-doped PAN systems studied here. The temperature dependence of σ_{dc} of the systems follows a quasi-one-dimensional variable range hopping model, which is similar to that of HCl-doped PAN samples. As the molar concentration increases from $\sim 10^{-4}M$ to $\sim 1M$, the system is transformed from an insulating to conducting (non-metallic) state. From EPR experiments, we measure the temperature dependence of magnetic susceptibility, and obtain the density of states for various Li-salt-doped PANs with different doping levels. We observe the increase of the density of states as the molar concentration increases. From the analysis of nitrogen 1*s* peak obtained from XPS experiments, we estimate the doping level of the systems. We compare the effective doping thickness between HCl-doped PAN samples and Li-salt-doped PAN ones, based upon the results of XPS argon (Ar) ion sputtering experiments. The diffusion rate of Li^+ or counterions and the dissociation constants of Li salt in doping solution play an important role for the effective doping and transport properties of the Li-salt-doped PAN samples.

DOI: 10.1103/PhysRevB.64.035101 PACS number(s): 72.80.Le, 71.20.Rv, 71.30.+h

I. INTRODUCTION

Polyaniline (PAN) has been intensively studied for the past decades.[1–9] The conducting form of PAN is obtained by a protonic acid such as hydrochloric acid (HCl) doping. The electronic structure of PAN has been investigated to understand the transformation from the insulating state to conduction state.[5,10,11] Epstein *et al.* reported the insulator-metal transition of PAN systems as a function of protonation level based upon the result of the increase of the Pauli susceptibility.[5] MacDiarmid and co-workers showed a similar transition from the result of dc conductivity (σ_{dc}), where σ_{dc} at room temperature (RT) varied from $\sim 10^{-10}$ to ~ 1 S/cm as the protonation level increases.[3] The protonic acid dopants such as HCl, HF, H_3PO_4, $HClO_4$, H_2SO_4, HNO_3, and HBF_4 have been used to obtain the conducting form of PAN.[1,10–14] The effect of moisture on PAN has also been studied.[15–17] Cao *et al.* reported PAN doped with various functionalized acids such as dodecylbenzenesulfonic acid (DBSA) and camphorsulfonic acid (CSA). The σ_{dc} of PAN-CSA prepared in *m*-cresol solvent is $\geqslant 100$ S/cm, and its temperature dependence has an intrinsic metallic nature from RT to ~ 200 K.[18] Monkman and co-workers studied the reaction conditions at low temperature to synthesize the high-molecular-weight and highly conducting PAN materials.[19] The PAN samples doped with 2-acrylamido-2-methyl sulfonated propanoic acid (PAN-AMSPA) shows σ_{dc}(RT) ~ 400 S/cm reported by Lee *et al.*[20] The physical and chemical properties of PAN doped with protonic acid vary with the solvents (*m*-cresol, NMP, $CHCl_3$, etc.).[21,22] Based upon the protonic acid doping, various dopants and solvents have been used to increase and to control the σ_{dc} of PAN systems. The intrinsic metallic nature of doped PAN samples including polyacetylene and polypyrrole has been also studied through low temperature (below 10 K) σ_{dc} and optical dielectric constant as a function of energy.[9,23] However, there have been many controversial issues in the intrinsic metallic nature and details of charge transport mechanisms.[9]

The PAN materials can be used for electrodes of lithium (Li) ion rechargeable batteries,[24] corrosion protection,[25] and rf and microwave absorbers.[26] The commercial use of PAN materials for batteries has begun with Bridgestone Corporation and Seiko Electronic Components Ltd.[27] The electrochemical redox reactions using the emeraldine base form of PAN (PAN-EB) and the use of PAN as a cathode in a rechargeable battery has been studied.[28] PAN materials doped with Li salts and their composites are promising candidates for electrodes of Li ion rechargeable batteries, because they are stable in air, have relatively high conductivities, and are compatible with polymer electrolytes.[1,2]

In this study, we synthesize PAN samples doped with various Li salts ($LiPF_6$, $LiBF_4$, $LiAsF_6$, $LiCF_3SO_3$, or $LiClO_4$). Electrical, magnetic, and structural properties of Li-salt-doped PAN samples are compared with those of HCl-doped emeraldine salt forms of PAN (PAN-ES) through the temperature dependence of σ_{dc} and thermoelectric power, electron paramagnetic resonance (EPR), and X-ray photoelectron spectroscopy (XPS) experiments. We discuss the in-

homogeneous doping of the systems based on EPR and XPS Ar sputtering experiments.

II. EXPERIMENT

The powder of a PAN-EB (PANIPOL™, NESTE, Finland) was dissolved in *N*-methylpyrrolidinone (NMP) solvent, and its weight ratio was 3% with respect to the solvent. The solution was stirred with spin bars for 24 h and filtered with Watman filter paper three times. The solution was poured on a slide glass and dried at 50 °C in a convection oven under the dynamic vacuum for 15 h to prepare a PAN-EB free-standing film. For the doping solution of the Li salts, ethylene carbonate (EC, $C_3H_4O_3$, molecular weight $\cong$88.06, density$\cong$1.32 g/cm^3) and dimethyl carbonate [DMC, $(CH_3O)_2CO$, molecular weight$\cong$90.08, density $\cong$1.07g/cm^3] were used as the solvents. The PAN-EB free-standing films were immersed in the Li-salt-doping solution for 72 h, and the doping process was performed in a dry box. The doped films were dried in vacuum oven at 50 °C for 15 h and washed with ethyl ether.

The σ_{dc} was measured by using a four-probe method, in order to eliminate the contact resistance. A CTI-Cryogenics closed-cycle refrigerator system was used for measuring the temperature dependence of dc conductivity $[\sigma_{dc}(T)]$ from RT to ~20 K. For low-temperature dc conductivity measurements from 70 K to 3 K, the physical property measurement system (PPMS) Keithley model 7065 Hall effect card were used. A Brucker ESP 300 spectrometer (*X* band) was used to obtain the EPR spectra. The samples were put in an EPR tube (Wilmad 707) and pumped with a diffusion vacuum pump ($\leqslant 10^{-5}$ Torr) before sealing the tube to avoid the possible air and moisture effects on the EPR signal of samples. The magnetic susceptibilities of the system were estimated from EPR integrated intensities calibrated against a Li-LiF crystal. The XPS data were measured by using a PHI 5700 spectrometer (Al $K\alpha$, 1486.7 eV photons). The carbon 1*s* (C ls) neutral peak at 284.6 eV was used as the reference to correct for the shift caused by surface-charging effects.[29,30] The XPS sputtering on the surface of PAN samples was performed by using Ar ions (3 keV) for 10 min under 10^{-7} Torr.

III. EXPERIMENTAL RESULTS

A. dc conductivity and thermoelectric power

Figure 1 compares $\sigma_{dc}(T)$ for PAN-ES and Li-salt-doped PAN samples. The σ_{dc}(RT) of PAN-ES and PAN doped with $LiPF_6$ (PAN-$LiPF_6$) is ~10 S/cm and ~1 S/cm, respectively. The σ_{dc}(RT) and its temperature dependence of Li-salt-doped PAN samples vary with the kind of dopants used as shown in Fig. 1. PAN-$LiPF_6$ has the highest σ_{dc}(RT) in Li-salt-doped PAN systems studied here. A quasi-one-dimensional (1D) variable range hopping (VRH) model provides the best fitting for $\sigma_{dc}(T)$ of PAN-ES and Li-salt-doped PAN systems. The quasi-1D VRH model emphasizing the nearest-neighboring interchain hopping has been used to account for the macroscopic dc charge transport of PAN-ES samples,[31] which is described as

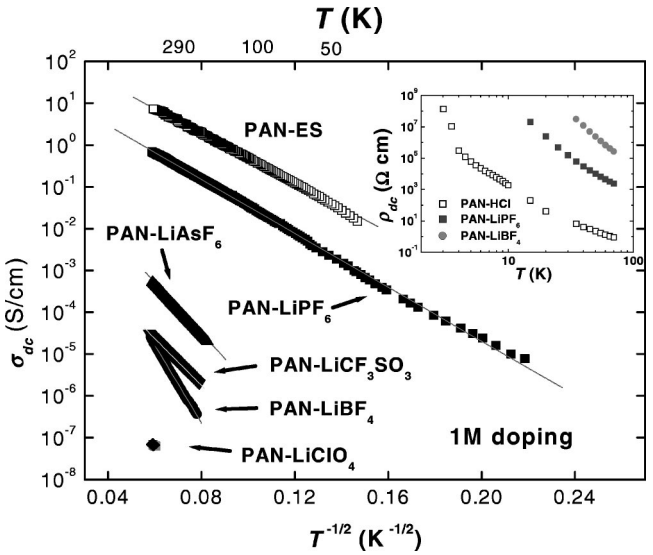

FIG. 1. Temperature dependence of σ_{dc} of PANs doped with various Li salts and HCl doped (PAN-ES) PAN samples. Inset: Temperature dependence of resistivity $[\rho_{dc}(T)]$ at low temperatures.

$$\sigma_{dc} = \sigma_0 \exp\left[-\left(\frac{T_0}{T}\right)^{1/2}\right], \tag{1}$$

where $T_0 = 16/[k_B N(E_F) L_\parallel L_\perp^2]$, $N(E_F)$ is the density of states at the Fermi level, and $L_\parallel$ ($L_\perp$) is the localization length in the parallel (perpendicular) direction.[32,33] The slope of $\sigma_{dc}(T)$, T_0 can be interpreted as an effective energy barrier or energy difference between localized states. The results of $\sigma_{dc}(T)$ imply that the quasi-1D structure for charge transport maintains for Li-salt-doped PAN systems. The T_0 values of the PAN-$LiPF_6$, PAN-$LiAsF_6$, PAN-CF_3SO_3, and PAN-$LiBF_4$ samples are ~5400 K, 19 000 K, 21 000 K, and 46 000 K, respectively. The PAN-$LiPF_6$ sample is the most highly conducting sample in the Li-salt-doped PAN samples studied here. Assuming that $L_\parallel L_\perp^2 \simeq L^3$ and using the density of states $[D(E_F)]$ obtained from EPR experiments, the localization length (L) is estimated to be 23 Å, 22 Å, and 16 Å for PAN-$LiPF_6$, PAN-$LiAsF_6$, and PAN-$LiBF_4$, respectively. This suggests that the PAN-$LiBF_4$ sample is a relatively more localized state than the PAN-$LiPF_6$ sample. It is noted that $\sigma_{dc}(T)$ varies with Li-salt dopants used, although the systems are doped in the same $1M$ concentration of dopant. The inset of Fig. 1 represents the temperature-dependent resistivity $[\rho_{dc}(T)]$ at low temperatures. We observed that ρ_{dc} goes to infinity as temperature decreases due to disorder. This implies that the systems are not typical metals.

Figure 2 shows the variations of σ_{dc}(RT) of PAN-ES, PAN-$LiPF_6$, and PAN-$LiBF_4$ samples as a function of molar concentration. For PAN-$LiPF_6$ samples, we observe the increase of σ_{dc}(RT) from $\sim 10^{-9}$ S/cm to ~1 S/cm as the molar concentration increases from $10^{-4}M$ to $1M$. The σ_{dc}(RT) of PAN-$LiBF_4$ samples varies $\sim 10^{-9}$ S/cm to $\sim 10^{-4}$ S/cm as the molar concentration increases from $10^{-4}M$ to $1M$. This transformation from insulating state to conducting (non-metallic) state of PAN-$LiPF_6$ samples is

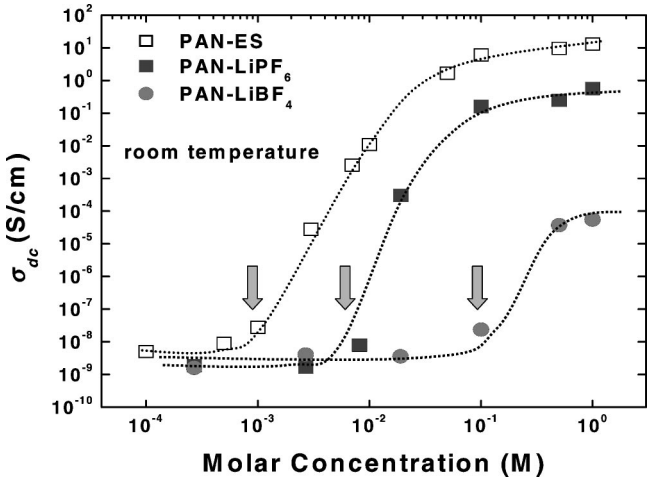

FIG. 2. The variation of σ_{dc}(RT) of PAN samples doped with HCl, $LiPF_6$, and $LiBF_4$, as a function of molar concentration. The dotted lines are for eye-guide. The downward arrows represent the onset of the transition.

similar to that of PAN-ES samples. However, for PAN-$LiPF_6$ and PAN-$LiBF_4$ samples, the onset of the transformation appears at $\sim 10^{-2}M$, and $\sim 10^{-1}M$, respectively, while that of PAN-ES samples appears at $\sim 10^{-3}M$, as the downward arrows shown in Fig. 2. The results indicate that the transformation from insulating state to conducting state of PAN systems easily occurs in the protonation doping process, rather than in the Li-salt-doping process. For Li-salt-doped PAN samples, the onset of that transformation varies with dopants used.

The temperature dependence of thermoelectric power (S) of PAN-$LiPF_6$ ($1M$) is shown in Fig. 3. The thermoelectric power of the PAN-$LiPF_6$ sample linearly increases as the temperature increases above 150 K. The sign of thermoelectric power of the PAN-$LiPF_6$ sample is positive above 150 K, which implies the hole transport of the system. The negative thermoelectric power and the nonlinearity at low temperatures ($\leqslant$150 K) are mainly due to the contribution of charge transport characteristics of the quasi-1D VRH.[33]

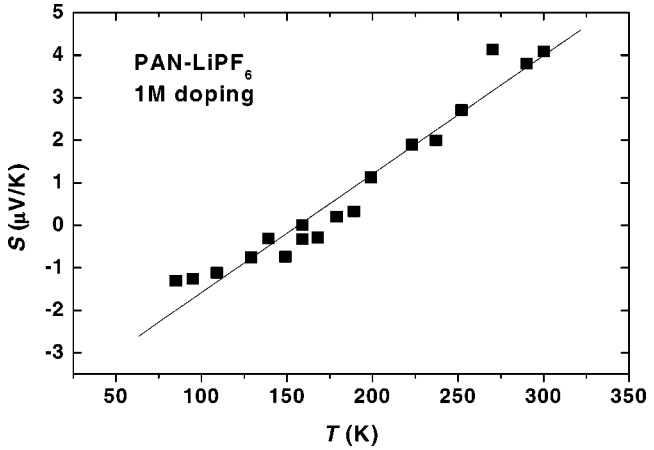

FIG. 3. Temperature dependence of thermoelectric power of PAN-$LiPF_6$ samples.

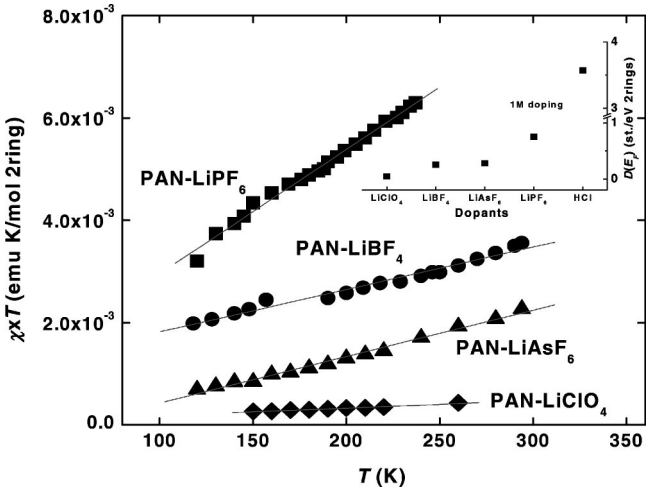

FIG. 4. $\chi \times T$ vs T for various Li salt doped PAN samples. Inset: the density of states $[D(E_F)]$ of PAN-ES and various Li salt doped PAN samples.

B. Electron paramagnetic resonance (EPR)

Figure 4 compares temperature dependence of the magnetic susceptibility (χ) of various Li-salt-doped PAN samples obtained from EPR experiments. Assuming that total magnetic susceptibility (χ) is composed of the Pauli (χ^P, which is independent of temperature), and Curie ($\chi^C = C/T$ where C is the Curie constant) components, linear fitting of χT against the temperature provide χ^P.[6] The slope (χ^P) for the PAN-$LiPF_6$ sample is larger than that for the other Li-salt-doped PAN samples as shown in Fig. 4. The χ^P is due to free conduction electrons, while the χ^C has the nature of localized spins. Therefore, the PAN-$LiPF_6$ sample is the highest conducting state in the Li-salt-doped PAN samples studied here, which is in accordance with the results of $\sigma_{dc}(T)$. The inset of Fig. 4 presents the density of states $[D(E_F)]$ of PAN-ES and Li-salt-doped PAN samples. Using the relation $\chi^P = \mu_B^2 D(E_F)$, where μ_B is the Bohr magneton, the density of states of PAN-$LiPF_6$, PAN-$LiAsF_6$, PAN-$LiBF_4$, and PAN-$LiClO_4$ samples is estimated to be 0.75, 0.28, 0.26, and 0.046 states/(eV two rings), respectively. We observe that the $D(E_F)$ varies with the dopants used as shown in the inset of Fig. 4. The relatively low $D(E_F)$ of Li-salt-doped PAN samples compared to that of conventional PAN-ES samples suggests that Li-salt-doped PAN samples are in the inhomogeneously doped state.

The variation of the $D(E_F)$ as a function of molar concentration for PAN-$LiPF_6$ and PAN-$LiBF_4$ samples is shown in Fig. 5. $D(E_F)$ is calculated by using the relation $\chi^P = \mu_B^2 D(E_F)$. $D(E_F)$ increases as the doping level increases. The sudden increase of the $D(E_F)$ for PAN-$LiPF_6$ and PAN-$LiBF_4$ samples is observed at $\sim 10^{-2}M$ and $\sim 10^{-1}M$, respectively, as the downward arrows shown in Fig. 5. These results agree with the transformation from insulating state to conducting state observed in σ_{dc}(RT).

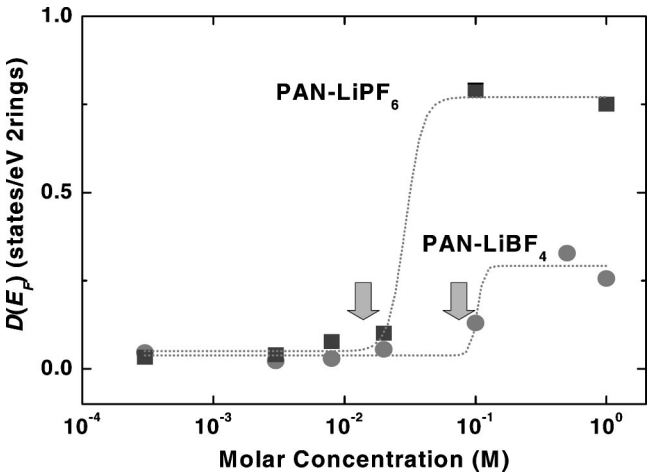

FIG. 5. The variation of the density of states $[D(E_F)]$ as a function of molar concentration for PAN-$LiPF_6$ and PAN-$LiBF_4$ samples. The dotted lines are for eye-guide.

Figure 6 shows the doping level dependence of the χ^P for the PAN-$LiPF_6$ and PAN-$LiBF_4$ samples. The χ^P of the PAN-$LiPF_6$ and PAN-$LiBF_4$ samples increases as the doping level increases. The relatively small χ^P of Li-salt-doped PAN systems compared to that of PAN-ES ($\chi^P = 12\times10^{-5}$ emu/mol 2 rings) is expected from the inhomogeneous doping in Li salts doped PAN systems. We can describe χ^P as a step function,

$$\chi^P(y) = (1/2)\chi_0\left[1+\tanh\left(\frac{y-y_0}{\Delta y}\right)\right], \tag{2}$$

where $\chi_0 = \mu_B^2 D(E_F)$, y is the doping level, Δy is the sharpness of the step, and $\chi^P(y_0) = \chi_0$.[34,35] From the comparison of the EPR signal intensity aganist the standard sample, the free spin exists per 20 rings for the PAN-$LiPF_6$ sample ($1M$), and per 50 rings for the PAN-$LiBF_4$ sample ($1M$). These values are smaller than the results of XPS experiments. In order to account for this discrepancy due to the inhomogeneous doping, we assume that

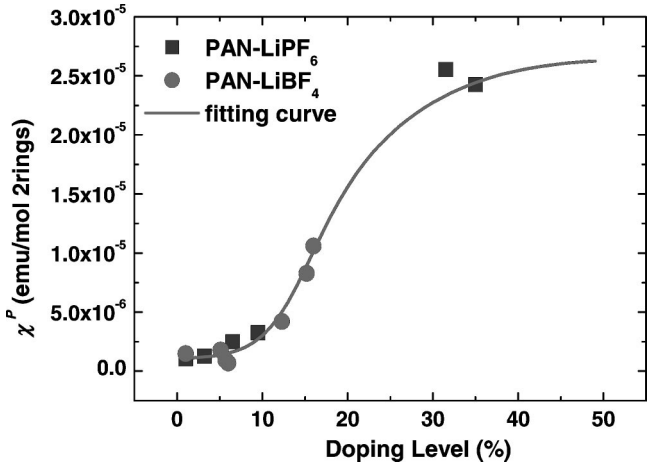

FIG. 6. χ^P (scattered markers) and χ_m^P (solid line) vs doping level for PAN-$LiPF_6$, and PAN-$LiBF_4$ samples. The fitting curve is based on Eq. (4).

$$y = y_{\max}\exp\left(\frac{-x^2}{4D\tau}\right). \tag{3}$$

Here $y_{\max}$ is the maximum doping level, which is related to the molar concentration and dissociation constant of the dopant, x is the diffusion distance, D is the diffusion constant, and τ is the minimum doping time for the saturation. The Eq. (3) is based on the assumption that the amount of the dopant decreases toward the inside of the sample. From Eqs. (2) and (3), we can obtain the theoretical Pauli susceptibility (χ_m^P) in the case of inhomogeneous doping by using the following equation,

$$\chi_m^P(y) = \frac{4}{d}\int_0^{d/2}\chi^P(y)\,dx + \chi_1$$

$$= \frac{4}{d}\int_0^{d/2}\chi_0\left[1+\tanh\left(\frac{y-y_0}{\Delta y}\right)\right]dx + \chi_1, \tag{4}$$

where d is the thickness of the sample and χ_1 is the Pauli susceptibility when y is 0. The χ_m^P obtained from the computer simulation using Eq. (4) is presented by the solid fitting curve in Fig. 5. We used $y_0 = 14\%$, $\chi_0 = 13\times10^{-6}$ emu/(mol 2 rings), $\Delta y = 4.8\%$, and $\chi_1 = 1.0\times10^{-6}$ emu/(mol 2 rings) for the best fitting. The analysis of Fig. 6 suggests that the transformation from insulating state to conducting state can be explained by the diffusion of Li salts through PAN samples.

Figure 7(a) shows temperature dependence of EPR linewidth $[\Delta H_{p\text{-}p}(T)]$ of PAN-$LiPF_6$ samples with different doping levels. The $\Delta H_{p\text{-}p}$ of conducting PAN-$LiPF_6$ samples with $1M$ and $10^{-1}M$ concentrations linearly increases as temperature increases. However, for the insulating PAN-$LiPF_6$ samples with $2\times10^{-2}M$ and $8\times10^{-3}M$ concentrations, the $\Delta H_{p\text{-}p}$ decreases as temperature increases indicating motional narrowing. As the molar concentration increases, the values of the $\Delta H_{p\text{-}p}$ at each temperature decrease. The line narrowing is due to the increase of the number of mobile spins i.e., the increase of polarons with increasing the doping level. Figure 7(b) presents temperature dependence of the g values. The g value of the PAN-$LiPF_6$ and PAN-$LiBF_4$ samples are ~2.00292 and ~2.00317, respectively, which are almost independent of temperature from 100 K to RT. It is noted that the principle g value in π-electron radicals from the free-spin value is 2.0023. The deviation of g value is associated with spin-orbit interaction between the ground-state and excited-state radicals.[36]

C. X-ray photoelectron spectroscopy (XPS)

Figure 8 presents nitrogen 1s (N 1s) XPS core level spectra of PAN-ES and Li-salt-doped PAN samples at RT. The N 1s XPS peak line is decomposed into three peak lines as shown in Fig. 8. The FWHM (full width at half maximum) of imine nitrogen (—N═) and amine nitrogen (—N—)

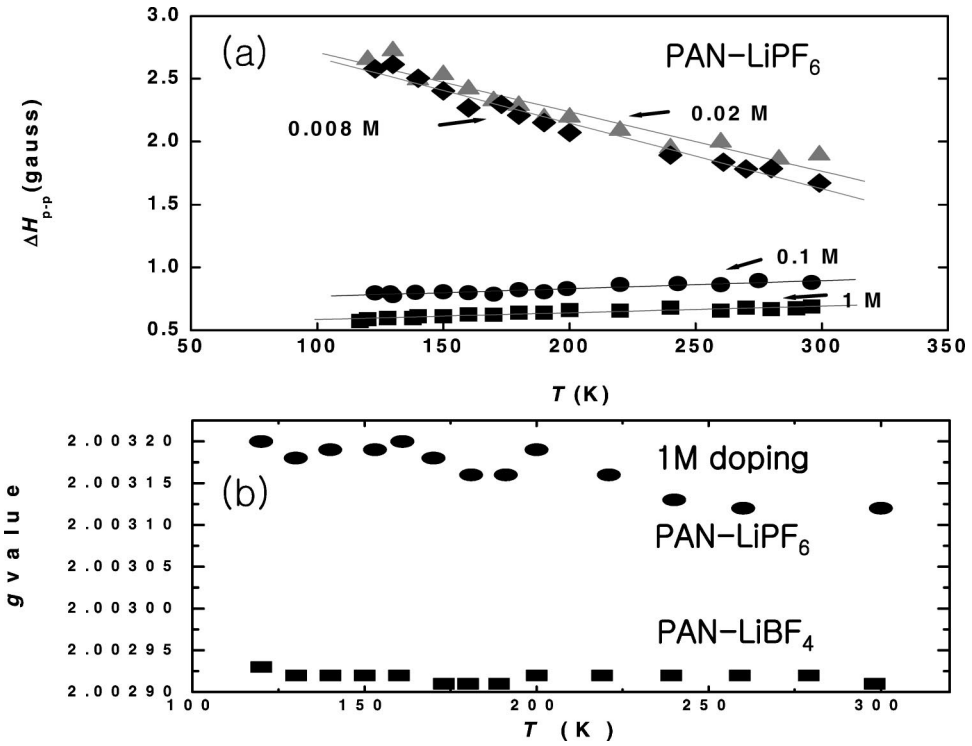

FIG. 7. Temperature dependence of (a) EPR peak to peak linewidth (ΔH_{p-p}) of PAN-$LiPF_6$ samples with different doping levels and (b) the g values of PAN-$LiPF_6$ and PAN-$LiBF_4$ samples.

peaks is maintained constant (1.65 eV). The lines due to imine nitrogen and amine nitrogen are centered at 398.1 ± 0.1 eV and 399.3 ± 0.1 eV, respectively.[29,30,37] The energy splitting between the imine nitrogen peak and the amine nitrogen peak is 1.2 eV. The error in the XPS curve fitting is ~5%. The percent of the area ratio of N^+ peak of PAN-$LiPF_6$ sample is ~35%, which is relatively larger than that of other Li-salt-doped PANs as shown in Fig. 8. The area ratio of N^+ peak centered at 401.0 ± 0.2 eV indicates the doping level of the Li-salt-doped PAN systems. The percent of area ratio of the N^+ component of the PAN-$LiPF_6$ samples is ~35%, which is similar to that (~32%) of PAN-ES samples. However, the area ratio of the N^+ component of other Li-salt-doped PAN samples except the PAN-$LiPF_6$ samples is less than 20%. The results suggest that the doping level varies with the kind of Li-salt dopants used, although the systems are doped in the same $1M$ concentration of dopant. The diffusion rate of Li^+ or counterions into the PAN-EB film and the degree of dissociation of a Li salt in the doping solution play an important role for the effective doping level.

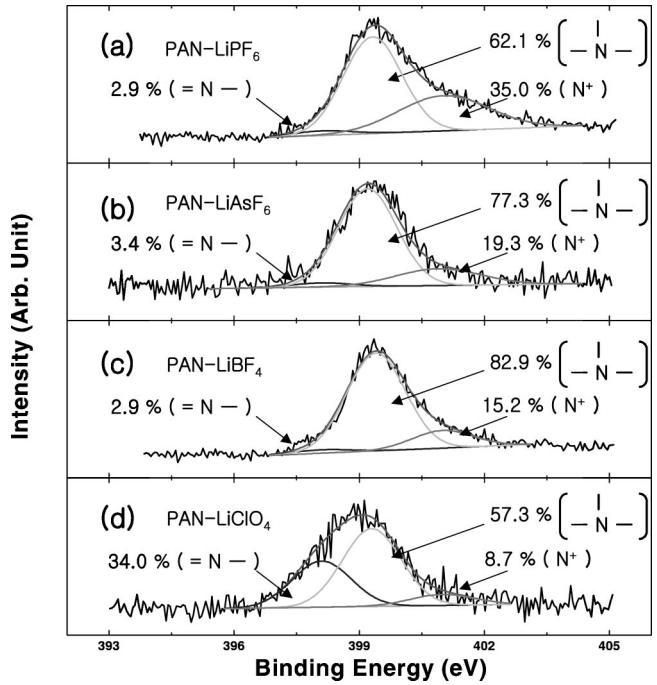

FIG. 8. Nitrogen 1s (N1s) XPS core level spectra for (a) PAN-$LiPF_6$, (b) PAN-$LiAsF_6$, (c) PAN-$LiBF_4$, and (d) PAN-$LiClO_4$ samples.

Figures 9(a)–9(d) compare the N 1s XPS core-level spectra for PAN-$LiPF_6$ samples with different molar concentrations. The percent of area ratio of the N^+ component increases with increasing molar concentration as shown in Fig. 9(e). These results qualitatively agree with the behavior of the transformation from insulating state to conducting state observed in σ_{dc}(RT) and the $D(E_F)$ as shown in Figs. 2 and 5.

IV. DISCUSSION

Figure 10 shows the variation of σ_{dc}(RT) as a function of doping time. The σ_{dc}(RT) of the PAN-$LiPF_6$ and PAN-$LiBF_4$ samples is saturated after ~10 h, while that of PAN-ES is saturated after ~30 min, as shown in Fig. 10. These results imply that the doping of PAN samples by using Li salts is relatively difficult compared to that of using protonic acid such as HCl. The size of Li^+ ion is relatively larger than proton to dope PAN samples homogeneously. We

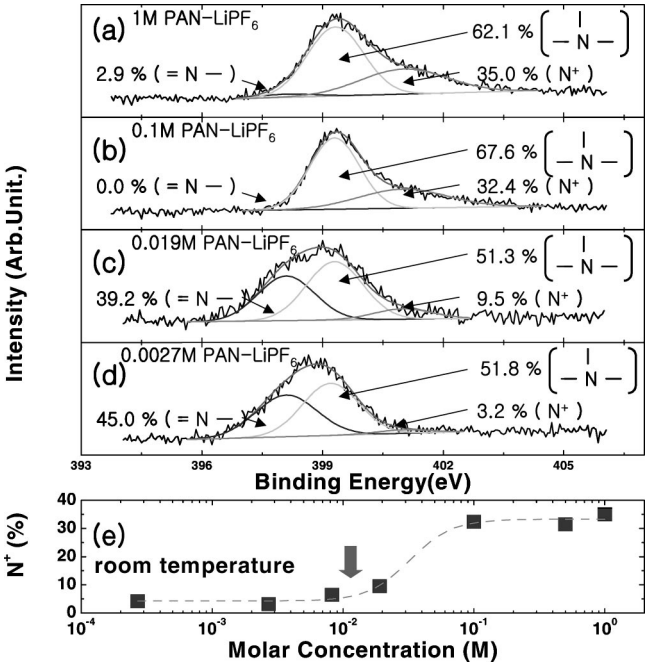

FIG. 9. N1s XPS core level spectra of PAN-$LiPF_6$ samples with different molar concentrations; (a) 1M, (b) 0.1M, (c) 0.019M, (d) 0.0027M, and (e) the variation of the percent of the area ratio of N^+ peak as a function of molar concentration for PAN-$LiPF_6$ samples.

assume that the process of Li-salt diffusion in PAN systems is the one-dimensional diffusion case, as follows:

$$C=(\alpha/\sqrt{t})\exp\left(\frac{-x^2}{4Dt}\right). \tag{5}$$

Here C, D, and α are the ion concentration, the diffusion constant, and the normalization constant, respectively.[38] The x and t are the diffusion distance and time, respectively.[38–40]

The diffusion coefficient, D is the function of the relaxation time (τ) considered as the minimum doping time for saturation and the sample thickness d, which is described as

$$D=\frac{(d/2)^2}{4\tau}. \tag{6}$$

The τ of the PAN-ES samples is ~30 min, while that of the PAN-$LiPF_6$ and the PAN-$LiBF_4$ samples is ~10 h. Therefore, the D of the PAN-ES samples ($\sim 9\times10^{-10}$ cm^2/s) is larger than the PAN-$LiPF_6$ and the PAN-$LiBF_4$ samples ($\sim 4\times10^{-11}$ cm^2/s). From Eq. (5), the ion concentration, C of the PAN-$LiPF_6$ and the PAN-$LiBF_4$ samples more rapidly decreases than PAN-ES samples as the diffusion distance (x) increases. The atomic mass and radius of the proton, the Li^+ ion, and the counterions are important factors for the diffusion coefficient, which determines the effective doping level. The Li^+ ion is heavier and larger than the proton and is the inhomogeneous doping ion for organic systems. The solvation effect is expected from the EC and DMC solvents. These cause the inhomogeneous doping in Li-salt-doped PAN samples. For polyacetylene, Li salts were used as dopants to apply the material for the electrodes of Li ion rechargeable batteries.[39,40] When polyacetylene was electrochemically doped with Li salts, the inhomogeneous doping was pointed out by El-Khodary and Bernier.[40]

Figure 11 compares the normalized area of fluorine 1s (F 1s) core-level spectra of Li-salt-doped PAN samples and chlorine 2p (Cl 2p) level spectra of PAN-ES sample as a function of sputtering time. The surface of the samples was etched by the sputtering of Ar ion beam with the energy of 3 keV for 10 min. The normalized area of the F 1s XPS peak of the PAN-$LiPF_6$ and PAN-$LiBF_4$ samples is rapidly reduced after ~1 min, while that of the Cl 2p XPS peak of PAN-ES samples slowly increases and saturates as the sputtering time increases. The results indicate that the amount of

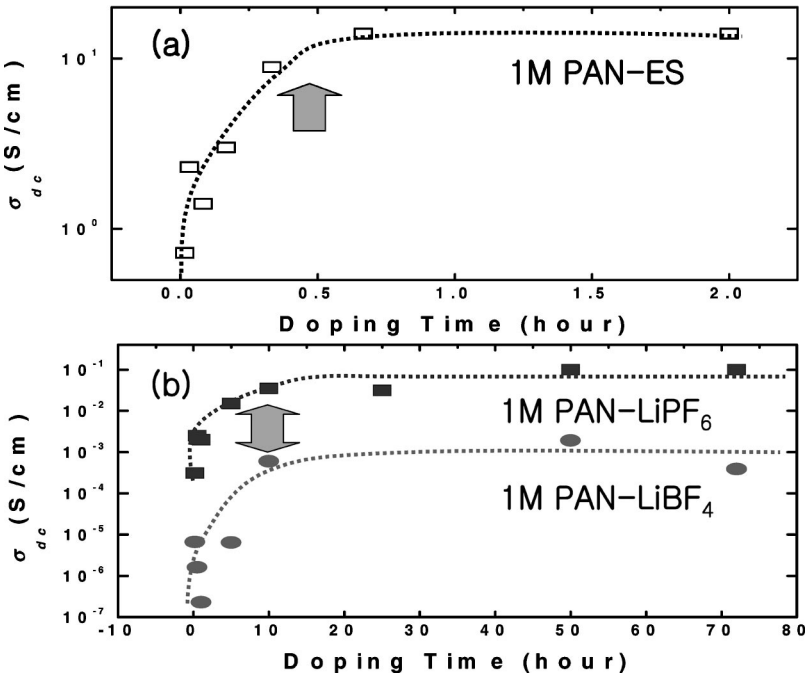

FIG. 10. The variation of σ_{dc} (RT) as a function of doping time for (a) PAN-ES and (b) PAN-$LiPF_6$ and PAN-$LiBF_4$ samples.

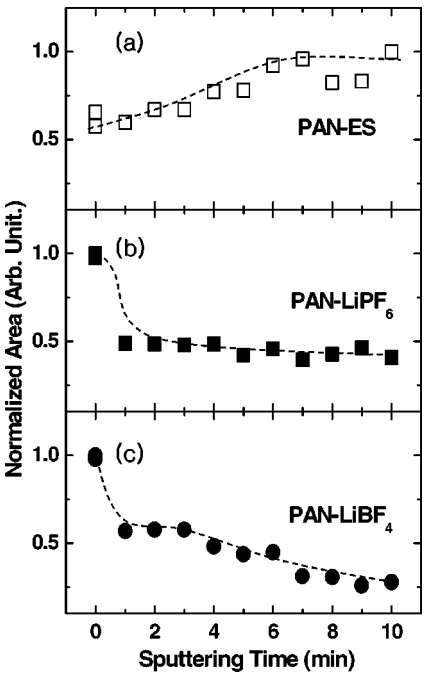

FIG. 11. The variation of the nomalized area of the counter ions (Cl2*p* and F1*s*) XPS peak of (a) PAN-ES, (b) PAN-$LiPF_6$, and (c) PAN-$LiBF_4$ samples.

Li^+ and counterions decreases toward the inside of the PAN-$LiPF_6$ and PAN-$LiBF_4$ samples. The relatively low area ratio of the Cl $2p$ XPS peak on the surface of PAN-ES samples in Fig. 11(a) is due to the volatile property of HCl or the washing process with ethyl ether.[30] The results imply that a relatively large amount of dopants or counterions exists on the surface of the PAN-$LiPF_6$ and PAN-$LiBF_4$ samples, and the distribution of Li^+ and counter ions is not uniform through the sample.

Based on the σ_{dc}, EPR, and XPS results, we suggest that the same doping process with the protonic acid doping in PAN systems can be applied to Li-salt-doped PAN samples. However, the PAN-EB film is less uniformly doped when Li salts are used as dopant. This analysis is supported by the relatively lower σ_{dc}(RT) and its wide variation ($10^{-5} \sim 1$S/cm) depending on the kind of Li salts used.

V. CONCLUSION

Electrical, magnetic, and structural properties of various Li-salt-doped PAN samples are studied. The $\sigma_{dc}(T)$ of the systems follows the quasi-1D VRH model, which is similar to that of PAN-ES samples. We observe that the samples with higher σ_{dc} have higher χ^P and the density of states. The σ_{dc}, its temperature dependence, and the density of states of Li-salt-doped PANs vary with the dopants used. From σ_{dc}(RT), the density of states, and the percent of the area ratio of the positive nitrogen as the functions of molar concentrations, we observe the transformation insulating state to conducting (non-metallic) state of the PAN-$LiPF_6$ sample. The molar concentration of the onset of the transformation for PAN-ES, PAN-$LiPF_6$, and PAN-$LiBF_4$ samples is $\sim 10^{-3}M$, $\sim 10^{-2}M$, $\sim 10^{-1}M$, respectively. We propose that the doping process in Li-salt-doped PAN systems is similar to that of protonic-acid-doped PAN system, i.e., the formation of polarons. However, Li-salt-doped PAN samples are inhomogeneously doped systems based on the results of EPR, XPS Ar ion sputtering, and time-dependent σ_{dc} experiments. The diffusion rate of the dopants into PAN-EB film samples plays an important role for the effective doping level and the doping thickness for the Li-salt-doped PAN systems.

ACKNOWLEDGMENTS

The authors wish to acknowledge the financial support of the KOSEF-CRM (2000) and the BK-21.

*Author to whom correspondence should be addressed. Electronic address: jjoo@mail.korea.ac.kr

[1] A.G. MacDiarmid, J.C. Chiang, M. Halpern, W. Huang, S. Mu, N.L.D. Somasiri, W. Wu, and S.T. Yaniger, Mol. Cryst. Liq. Cryst. **121**, 173 (1985).
[2] J.C. Chiang and A.G. MacDiarmid, Synth. Met. **13**, 193 (1986).
[3] A.G. MacDiarmid, J.C. Chiang, and A.F. Richter, Synth. Met. **18**, 285 (1987).
[4] F. Zuo, M. Angelopoulos, A.G. MacDiarmid, and A.J. Epstein, Phys. Rev. B **36**, 3475 (1987).
[5] A.J. Epstein, J.M. Ginder, F. Zuo, R.W. Bigelow, H.-S. Woo, D.B. Tanner, A.F. Richter, W.-S. Huang, and A.G. MacDiarmid, Synth. Met. **21**, 63 (1987).
[6] J.M. Ginder, A.F. Richter, A.G. MacDiarmid, and A.J. Epstein, Solid State Commun. **63**, 97 (1987).
[7] M.E. Jozefowicz, R. Laversanne, H.H.S. Javadi, A.J. Epstein, J.P. Pouget, X. Tang, and A.G. MacDiarmid, Phys. Rev. B **39**, 12958 (1989).
[8] L. Zuppiroli, M.N. Bussac, S. Paschen, O. Chauvet, and L. Forro, Phys. Rev. B **50**, 5196 (1994).
[9] R.S. Kohlman, J. Joo, Y.G. Min, A.G. MacDiarmid, and A.J. Epstein, Phys. Rev. Lett. **77**, 2766 (1996).
[10] W.R. Salaneck, I. Lundstrom, T. Hjertberg, C.B. duke, E. Conwell, A. Paton, A.G. MacDiarmid, N.L.D. Somasiri, W.S. Huang, and A.F. Richter, Synth. Met. **18**, 291 (1987).
[11] D. Vachon, R.O. Angus, Jr., F.L. Lu, M. Nowak, Z.X. Liu, H. Schaffer, F. Wudl, and A.J. Heeger, Synth. Met. **18**, 297 (1987).
[12] B. Wang, J. Tang, and F. Wang, Synth. Met. **18**, 323 (1987).
[13] K. Okabayashi, F. Goto, K. Abe, and T. Yoshida, Synth. Met. **1987**, 365 (1987).
[14] J.F. Rouleau, J. Goyette, T.K. Bose, R. Singh, and R.P. Tandon, Phys. Rev. B **52**, 4801 (1995).
[15] M. Angelopoulos, A. Ray, A.G. MacDiarmid, and A.J. Epstein, Synth. Met. **21**, 21 (1987).
[16] H.H.S. Javadi, M. Angelopoulos, A.G. MacDiarmid, and A.J. Epstein, Synth. Met. **26**, 1 (1988).
[17] P.K. Kahol, H. Guan, and B.J. McCormick, Phys. Rev. B **44**, 10393 (1991).
[18] Y. Cao, P. Smith, and A.J. Heeger, Synth. Met. **48**, 91 (1992).
[19] P.N. Adams, P.J. Laughlin, and A.P. Monkman, Synth. Met. **76**, 157 (1996).
[20] W.-P. Lee, K.R. Brenneman, A.D. Gudmundsdottir, M.S. Platz,

P.K. Kahol, A.P. Monkman, and A.J. Epstein, Synth. Met. **101**, 819 (1999).
[21] A.G. MacDiarmid, Arthur J. Epstein, Synth. Met. **65**, 103 (1994).
[22] J. Joo, Y.C. Chung, H.G. Song, J.S. Baeck, W.P. Lee, A.J. Epstein, A.G. MacDiarmid, S.K. Jeong, and E. J. Oh, Synth. Met. **84**, 739 (1997).
[23] T. Ishiguro, H. Kaneko, Y. Nogami, H. Ishimoto, H. Nishiyama, J. Tsukamoto, A. Takahashi, M. Yamaura, T. Hagiwara, and K. Sato, Phys. Rev. Lett. **69**, 660 (1992).
[24] E.M. Genies, A.A. Syed and C. Tsintavis, Mol. Cryst. Liq. Cryst. **121**, 181 (1985).
[25] R. Racicot, R. Brown, and S.C. Yang, Synth. Met. **85**, 1263 (1997).
[26] A. J. Epstein, A. G. Roe, J. M. Ginder, H. H. S. Javadi, and J. Joo, United States Patent Number 5,563,182, October, 8, 1996.
[27] T. Nakajima and T. Kawagoe, Synth. Met. **28**, C629 (1989).
[28] A.G. MacDiarmid, L.S. Yang, W.S. Huang, and B.D. Humphrey, Synth. Met. **18**, 393 (1987).
[29] K.L. Tan, B.T.G. Tan, E.T. Kang, and K.G. Neoh, Phys. Rev. B **39**, 8070 (1989).
[30] E.T. Kang, K.G. Neoh, and K.L. Tan, Prog. Polym. Sci. **23**, 277 (1998).
[31] N. F. Mott and E. Davis, *Electronic Processes in Non-Crystalline Materials* (Clarendon, Oxford, 1979).
[32] Z.H. Wang, C. Li, E.M. Scherr, A.G. MacDiarmid, and A.J. Epstein, Phys. Rev. Lett. **66**, 1745 (1991).
[33] Z.H. Wang, E.M. Scherr, A.G. MacDiarmid, and A.J. Epstein, Phys. Rev. B **45**, 4190 (1992).
[34] A.J. Epstein, H. Rommelmann, M.A. Druy, A.J. Heeger, and A.G. MacDiarmid, Solid State Commun. **38**, 683 (1981).
[35] M. Reghu, Y. Cao, D. Moses, and A.J. Heeger, Phys. Rev. B **47**, 1758 (1993).
[36] J.R. Morton, Chem. Rev. **64**, 453 (1964).
[37] S. Chen and L. Lin, Macromolecules **28**, 1239 (1995).
[38] W. Jost, *Diffusion in Solids, Liquids and Gases* (Academic Press, New York, 1960).
[39] F. Rachdi, P. Bernier, E. Faulques, S. Lefrant, and F. Schue, J. Chem. Phys. **80**, 6285 (1984).
[40] A. El-Khodary and P. Bernier, J. Chem. Phys. **85**, 2243 (1986).